Further morphological evidence on South African earliest Homo lower postcanine dentition: Enamel thickness and enamel dentine junction

Lei Pan, Jean Dumoncel, Frikkie de Beer, Jakobus Hoffman, John Francis Thackeray, Benjamin Duployer, Christophe Tenailleau, José Braga

Further morphological evidence on South African earliest *Homo* lower postcanine dentition: Enamel thickness and enamel dentine junction

Lei Pan [a, b, *], Jean Dumoncel [a], Frikkie de Beer [c], Jakobus Hoffman [c], John Francis Thackeray [d], Benjamin Duployer [e], Christophe Tenailleau [e], José Braga [a, d]

[a] *Computer-Assisted Palaeoanthropology Team, UMR 5288 CNRS-Université de Toulouse (Paul Sabatier), 37 Allées Jules Guesde, 31000 Toulouse, France*
[b] *Key Laboratory of Vertebrate Evolution and Human Origins of Chinese Academy of Sciences, Institute of Vertebrate Paleontology and Paleoanthropology, Chinese Academy of Sciences, 100044 Beijing, China*
[c] *South African Nuclear Energy Corporation, Pelindaba, North West Province, South Africa*
[d] *Evolutionary Studies Institute, University of the Witwatersrand, PO WITS, Johannesburg 2050, South Africa*
[e] *Centre Inter-universitaire de Recherche et d'Ingénierie des Matériaux, UMR 5085 CNRS-Université de Toulouse (Paul Sabatier), 118 route de Narbonne, 31062 Toulouse Cedex 9, France*

Keywords:
Australopiths
Geometric morphometric
Taxonomic discrimination
Dental evolution
Dietary adaptation

A B S T R A C T

The appearance of the earliest members of the genus *Homo* in South Africa represents a key event in human evolution. Although enamel thickness and enamel dentine junction (EDJ) morphology preserve important information about hominin systematics and dietary adaptation, these features have not been sufficiently studied with regard to early *Homo*. We used micro-CT to compare enamel thickness and EDJ morphology among the mandibular postcanine dentitions of South African early hominins ($N = 30$) and extant *Homo* sapiens ($N = 26$), with special reference to early members of the genus *Homo*. We found that South African early *Homo* shows a similar enamel thickness distribution pattern to modern humans, although three-dimensional average and relative enamel thicknesses do not distinguish australopiths, early *Homo*, and modern humans particularly well. Based on enamel thickness distributions, our study suggests that a dietary shift occurred between australopiths and the origin of the *Homo* lineage. We also observed that South African early *Homo* postcanine EDJ combined primitive traits seen in australopith molars with derived features observed in modern human premolars. Our results confirm that some dental morphological patterns in later *Homo* actually occurred early in the *Homo* lineage, and highlight the taxonomic value of premolar EDJ morphology in hominin species.

1. Introduction

Molar enamel thickness has provided information about hominin taxonomy, functional morphology, and dietary ecology (Kay, 1981, 1985; Martin, 1985; Ungar et al., 2006; Kono and Suwa, 2008; Smith et al., 2008; Olejniczak et al., 2008c). Although two-dimensional (2D) and three-dimensional (3D) studies of relative enamel thickness effectively distinguish between Neanderthals and modern humans (Olejniczak et al., 2008a; Bailey et al., 2014; Benazzi et al., 2015), enamel thickness has been shown to be homoplastic and does not consistently provide taxonomical information (Smith et al., 2003; Olejniczak et al., 2008b; Skinner et al., 2015). The utility of dental tissue proportion for the taxonomy of fossil hominins from 4 million years ago (Myr) to recent times is limited due to an insufficient number of detailed analyses and a poorly contextualized fossil record. It was also suggested that simple cross-sectional measurements did not reliably predict observed 3D patterns (Olejniczak et al., 2008b). To date, enamel thickness in specimens transitional to *Homo* (here referred to as early *Homo*) or attributed to premodern *Homo* (*H. erectus* or *H. ergaster*) has been measured largely from naturally fractured teeth (Beynon and Wood, 1986; White et al., 1994) or virtual 2D measurements based on medical computed tomography (CT; Schwartz, 1997) and micro-CT imaging (Smith et al., 2012; Skinner et al., 2015). Enamel thickness has been reported as being significantly thinner in early *Homo* than in *Paranthropus* (Beynon and Wood, 1986, 1987; Rozzi, 1998). More recently, virtual 2D measurements based on micro-CTs indicated that values obtained in

* Corresponding author.
E-mail address: lei.pan@univ-tlse3.fr (L. Pan).

http://dx.doi.org/10.1016/j.jhevol.2016.05.003

three early *Homo* molars from South Africa exceeded modern human ranges and were closer to the "hyper thick" *Paranthropus* condition (Smith et al., 2012). Also, 2D and 3D measurements both identified thinner enamel relative to dentine proportions in Neanderthal deciduous and permanent teeth, compared with modern humans (Olejniczak et al., 2008a; Fornai et al., 2014; Benazzi et al., 2015). It has therefore been concluded that molar enamel thickness is highly variable within the genus *Homo* (Smith et al., 2012).

Whole crown 3D distribution of molar enamel has been investigated in *Australopithecus africanus*, *Paranthropus robustus*, and modern humans with the use of micro-CT (Kono et al., 2002; Kono and Suwa, 2008; Olejniczak et al., 2008b, c; Suwa et al., 2009). These studies have suggested distinct patterns among some fossil hominin species, but data on whole-crown enamel distributions from Early to Middle Pleistocene fossil hominins come only from *Ardipithecus* (Suwa et al., 2009), *Au. africanus*, *P. robustus* (Olejniczak et al., 2008a, b), and *H. erectus* (Zanolli, 2015). Three-dimensional molar enamel distribution in australopiths is thickest over cusp tips, in contrast to recent humans, who have thicker enamel surrounding the cusp base (Olejniczak et al., 2008b).

Observations on the morphology at the enamel dentine junction (EDJ) of the postcanine dentition (Corruccini, 1987; Olejniczak et al., 2004, 2007; Skinner et al., 2009, 2010; Braga et al., 2010) have supplemented investigations made separately on enamel thickness distribution. Indeed, primate postcanine EDJ morphology carries useful taxonomic and phylogenetic information (Butler, 1956; Olejniczak et al., 2004, 2007; Skinner et al., 2008a, b), and can successfully discriminate between species and subspecies of chimpanzee (Skinner, 2008). Dentine horn height, crown height, cervix shape, and protostylid expression all preserve taxonomically relevant shape information in *Au. africanus* and *P. robustus*. These two taxa show similar 3D EDJ shape and inter-individual metameric trends along the molar dentition, but *P. robustus* preserves a marked reduction in the buccolingual breadth of the distal crown between M_2 and M_3, and a marked interradicular extension of the enamel cap in M_1 and M_2 (Skinner et al., 2008b). When compared to extant humans, the degree of intra-individual metameric variation is small in *Au. africanus*, as it is in *Pan* specimens (Hlusko, 2002; Braga et al., 2010). Moreover, in the *Au. africanus* EDJ, the protostylid crest extends mesially around the base of the protoconid dentine horn, whereas in *P. robustus* the crest seems to be located between the dentine horns of the protoconid and hypoconid (Skinner et al., 2009). Analysis of M_2 shape variation in australopiths, South African early *Homo*, modern humans, and Neanderthals using 3D geometric morphometric (GM) studies has indicated that enamel crown and cervical outlines are less taxonomically informative than outer and inner crown surfaces (Fornai et al., 2015).

The present work aims to investigate 3D aspects of EDJ shape variation and enamel distribution in mandibular postcanine dentition among South African early Pleistocene hominins and modern humans, with special reference to South African early *Homo*, to test their taxonomic value and to investigate taxonomically-sensitive features in early *Homo*. Our study is based on micro-CT data, GM analysis, and a comparative sample of *P. robustus*, *Au. africanus*, Neanderthals, and extant *H. sapiens*.

2. Materials and methods

2.1. Study sample

The focus of our analysis was mandibular postcanine dental material from three South African hominins, SKX 21204, SK 15, and SKX 257, that we regard to be early Pleistocene *Homo* specimens, attributed either to hominins transitional to *Homo* (e.g., *Homo habilis*) or unambiguously considered as premodern *Homo* (e.g., *H. erectus*; Wood, 2010). Currently, the older, East African *H. erectus* and *H. habilis* materials are not available for study by the authors, so this paper focuses only on South African early *Homo*, but it would be very worthwhile to enlarge the sample to include East African materials. We compared the early *Homo* sample with South African australopith permanent lower postcanines ($N = 41$) assigned to either *P. robustus* or *Au. africanus*, extant *H. sapiens* ($N = 45$), and European Neanderthals ($N = 16$). Our sample contained a number of antimeres, so analyses and interpretation were based on the sample shown in Table 1: when antimeres were available, the better-preserved side was used or, when antimeres were equally well-preserved, the right side was selected (i.e., antimeres were not averaged). Tooth-by-tooth enamel thickness data including antimeres are reported in the Supplementary Online Material (SOM) Table 1.

2.2. Micro-computed tomography

All South African hominin specimens (except for Sts 52) were scanned using the X-Tek (Metris) XT H225L industrial micro-XCT system at the South African Nuclear Energy Corporation (Necsa; Hoffman and de Beer, 2012). Most of the extant *H. sapiens* specimens (except for all the M_3s), along with the Montmaurin Neanderthal and one *Au. africanus* specimen (Sts 52) were scanned at the Institute for Space Medicine and Physiology (MEDES) of Toulouse with a Scanco Medical X-Treme micro-CT scanner. The extant human M_3s and Neanderthals from La Chaise were scanned by Arnaud Mazurier at the Centre de Microtomographie of the Université de Poitiers (equipment X8050-16 Viscom AG; camera 1004 × 1004). Micro-CT data of the Krapina Neanderthals were downloaded from the NESPOS Database (NESPOS database, 2015). Isometric voxel size ranged from 10 to 70 μm. Each specimen was segmented and measured in Avizo 8.0 (Visualization Sciences Group, www.vsg3d.com). Statistical analyses were conducted using R (R Development Core Team, 2012), except for the Kruskal–Wallis test with Connover's post hoc comparison, which was undertaken using BrightStat (Stricker, 2008).

2.3. 3D surface reconstruction

Micro-CT image stacks were imported for semi-automated (modules "magic wand" and "Threshold") and automated (module "Watershed") segmentations, surface reconstructions, and visualizations ("Colormap" option) of whole-crown enamel thickness distributions. The 3D outer enamel surfaces and EDJ surfaces (simplified to 100,000 faces) were calculated using the "unconstrained smoothing" parameter.

Most of our sample contains crowns with no or only slight signs of attrition; 13 teeth showing wear facets reaching the later phase of stage 2 according to Molnar (1971) were excluded from the analysis of enamel thickness. The degree of wear for each fossil specimen is listed in Table 1. On account of fractures, very small reconstructions were made prior to measurement. In the majority of cases, this involved only very minor additions of dental tissue. It is worth noting that the left dentition of Sts 18 showed a degree of distortion, but we managed to digitally reconstruct the enamel and dentine tissue in good order.

2.3.1. 3D map of whole-crown enamel distribution To investigate the 3D distribution of enamel, we applied the "colormap" option to visualize whole-crown enamel thickness (Kono et al., 2002). First, we computed the minimal distance from the occlusal to the EDJ surfaces through the "Surface distance" module on Avizo v8.0.

Table 1
Composition of the study sample.[a]

Specimen	P_3	P_4	M_1	M_2	M_3	Provenance		Age	Occlusal wear	Citation[b]
P. robustus										
SK 1				1		**Swartkrans**	Mb. 1, HR	1.80 ± 0.09 Ma–2.19 ± 0.08 Ma	1	1–2
SK 6	***1***	1	***1***	1	1		Mb. 1, HR	(Gibbon et al., 2014),	1–3	1–2
SK 23					1		Mb. 1, HR	2.31–1.64 Ma (Pickering et al., 2011)	2	3
SK 37				1			Mb. 1, HR		1	1
SK 843				***1***	1		Mb. 1, HR		2–3	1
SK 855					1		Mb. 1, HR		2	5
SK 61	1		1				Mb. 1, HR		1	3
SK 63	1		1	1			Mb. 1, HR		1	1
SKW 5		***1***		1	1		Mb. 1, HR		1-late 2	6
SKX 4446		1	***1***	1			Mb. 2	1.36 ± 0.69 Ma (Balter et al., 2008)	1–3	4
TM 1517b					1	**Kromdraai B**	Unprovenanced	~1.9 Ma (Thackeray et al., 2002, 2005)	1	7–8
TM 1600					1		Unprovenanced		2	5, 8
Au. africanus										
Sts 18		1	***1***			**Sterkfontein**	Mb. 4	3.0–2.5 Ma (White and Harris, 1977;	2	1
Sts 52	***1***	***1***		1	1		Mb. 4	Tobias, 1978; Clarke, 1994), 2.8–2.4 Ma (Vrba, 1985; but see; Berger et al., 2002), 2.1 ± 0.5 Ma (Schwarcz et al., 1994)	2–3	1
Early *Homo*										
SKX 21204	1	1				**Swartkrans**	Mb. 1, LB	1.80 ± 0.09 Ma–2.19 ± 0.08 Ma (Gibbon et al., 2014), 2.31–1.64 Ma (Pickering et al., 2011)	1	4
SK 15				***1***	1		Mb. 2	1.36 ± 0.69 Ma (Balter et al., 2008)	2–3	9
SKX 257			1				Mb. 2		1	4
Extant *H. sapiens*	4	3	10/***2***	6	4	**Strasbourg University/Muséum National d'Histoire Naturelle**			1-late 2	10
Neanderthals										
Mandible 1					1	**Montmaurin**		~400 Ka (Girard, 1973)	1	11–12
S 5			1			**La Chaise**	Abri Suard	OIS 6 (Macchiarelli et al., 2006)	Early 2	13
S 14-7			1				Abri Suard		Early 2	13
S 49			1				Abri Suard		Early 2	13
BDJ4C9			***1***				Abri Bourgeois	OIS 5e (Macchiarelli et al., 2006)	Late 2	13–14
D1				***1***		**Krapina**	Level 8	OIS 5e (Rink et al., 1995)	Early 3	15–16
D6				1			Level 8		1-early 2	15–16
D7					1		Level 8		1-early 2	15–16
D10				1			Level 8		1-early 2	15–16
D80			1				Level 8		1-early 2	15–16
D85					1		Level 8		1-early 2	15–16
D86				1			Level 8		1-early 2	15–16
D105			1				Level 8		1-early 2	15–16
D106					1		Level 8		1-early 2	15–16
D107				1			Level 8		1-early 2	15–16
D108					1		Level 8		1-early 2	15–16

[a] Segmentation of all Sterkfontein and Kromdraai B samples and some of the modern human samples was done by JB, the others were done by LP. All 3D virtual images of the Neanderthal specimens were provided by Dr. C. Zanolli (NESPOS database, 2015). In each specimen, dental position(s) marked in bold and italic were only used in EDJ geometric morphometric studies because of wear; the wear stage is estimated according to (Molnar, 1971). It should be noted that our fossil hominins from Kromdraai B (KB) were not recovered from a single stratigraphic unit and the majority of those discovered before the 1970s, including the two KB *P. robustus* specimens in our sample (TM 1517 and TM 1600), are of unknown stratigraphic origin (Brain, 1975; Braga et al., 2013). However, the discovery of a provenanced left humerus shaft fragment (KB 5522), possibly associated with TM 1517g (Thackeray et al., 2005), indicates that this latter KB specimen could derive from the youngest KB hominin-bearing deposits.

[b] (1) Robinson (1956), (2) Broom (1949), (3) Broom and Robinson (1952), (4) Grine (1989), (5) Brain (1981), (6) Grine and Daeglin (1993), (7) Broom (1938), (8) Thackeray et al. (2001), (9) Broom and Robinson (1949), (10) Rampont (1994), (11) Billy and Vallois (1977a), (12) Billy and Vallois (1977b), (13) Debénath (1977), (14) Macchiarelli et al. (2006), (15) Radovčić et al. (1988), (16) NESPOS database (2015).

The distances were then visualized at the outer enamel surface using a color scale ranging from dark blue ("thinner") to red ("thicker").

2.3.2. Three-dimensional measurements of enamel thickness Our results and discussion of enamel thickness are based on data yielded from the 3D-b method described by Benazzi et al. (2014) to separate the crown from the root(s); the crown was separated from the root(s) based on the cervical line, and the coronal dentine tissue was sealed by a smooth surface following the curve of the cervical line ("Fill hole" option on Avizo 8.0). As the protocol set by Olejniczak et al. (2008c) has been widely used in previous studies of 3D enamel thickness (e.g., Olejniczak et al., 2008b; Zanolli et al., 2010; Zanolli, 2015), and one might be interested in a comparative study of the method, we also used the section plane defined by Olejniczak et al. (2008c) to separate the crown from the roots in our molar sample; this dataset is available in SOM Table 2. As described by Olejniczak et al. (2008c), we first located the most apical plane of the cervical section showing a continuous ring of enamel (plane A). We defined this plane by selecting three landmarks located along the cervical line with the farthest distances to the root; next, plane A was moved gradually toward the roots until the most apical section plane still containing enamel was located (plane B). The plane exactly halfway between planes A and B was taken as the cervical plane, above which coronal measurements were recorded.

Three variables were measured for each specimen: the volume of the enamel cap (Ve, mm^3), the volume of the coronal dentine that includes the volume of the coronal pulp (Vcdp, mm^3), and the surface area of the enamel dentine junction (SEDJ, mm^2). We then calculated two indices of enamel thickness: 3D AET (Ve/SEDJ), the 3D average enamel thickness (mm), and 3D RET ($100 \times$ 3D AET/$(Vcdp^{1/3})$), the scale-free 3D relative enamel thickness (Kono, 2004; Olejniczak et al., 2008a).

2.4. Geometric morphometrics

In some cases, especially in fossil specimens, only a tooth from one side was preserved (details in Table 1). Any image data from the left side were flipped to obtain a homogeneous right sided sample. For each tooth, we defined a set of landmarks as well as a set of semi-landmarks along the marginal ridge between the main dentine horns (DHs) as an approximation of the marginal ridge (Fig. 1). For premolars, the landmarks were placed on the tips of the DHs (i.e., 1. protoconid, 2. metaconid; numbered red circles in Fig. 1), with 55 semi-landmarks (30 and 15 along the distal and mesial marginal ridges, respectively, and 10 on the transverse crest that connects the two DHs). The molar landmark set included four landmarks on the tips of the DHs (i.e., 1. protoconid, 2. metaconid, 3. entoconid, 4. hypoconid; all marked with numbered red circles in Fig. 1), with 60 semi-landmarks forming a continuous line beginning at the tip of the protoconid and moving in a clockwise direction. All semi-landmarks were slid along their respective curves, which were separated by the main landmarks.

2.5. Statistical analyses

Differences in the distribution of 3D AET and RET between groups were tested using the rank-based Kruskal–Wallis test with Conover's post hoc comparisons (see SOM Table 3 for details). Summary and boxplots of 3D AET and RET in each taxon are shown in Table 2 and Figure 2. The GM analysis was conducted using R (R Development Core Team, 2012; packages ade4, scatterplot3d, and shapes). A Generalized Procrustes Analysis (GPA) was performed, and between-group PCAs (bgPCA) were undertaken to explore EDJ morphometric variations between groups (Mitteroecker and Bookstein, 2011; Gunz et al., 2012; Braga et al., 2013). The first two axes were plotted in order to visualize the shape distribution of each group and the overall shape variation.

3. Results

3.1. 3D enamel thickness and distribution

Average and relative enamel thickness (3D AET and RET) values are given in Table 2 and Figure 2 for each species (detailed in SOM Table 1). There was considerable overlap of 3D RET among the groups, regardless of dental position. However, only a minor overlap of 3D AET was observed between South African hominin groups and modern human/Neanderthals. Nonparametric tests revealed significant differences in premolar 3D RET and molar 3D AET and RET among the taxa. Conover's post hoc tests further highlighted distinctions between *P. robustus*, extant humans, and Neanderthals. Extant human premolars have significantly thinner 3D RET than *P. robustus*. Extant human molars have significantly thinner 3D AET than *P. robustus*, but significantly thicker 3D RET than Neanderthals. Also, Neanderthal molars showed significantly thinner 3D AET and RET than *P. robustus* (SOM Table 3). Our early *Homo* M_3 (SK 15) has moderately worn cusp tips but no dentine exposure; we report its enamel thickness because it represents a group with a scarce fossil record, but interpretation of enamel thickness based on such specimens should be undertaken with caution.

Figures 3–6 present the enamel thickness distribution color maps of the best-preserved postcanine dentition of the early *Homo*, australopiths, and extant humans and the molar dentition of Neanderthals, which because of their preservation are most likely to represent accurately the enamel thickness distribution pattern of each taxon. The rest of the color maps are shown in SOM Figures 1–4. In general, the australopith lower post-canines have

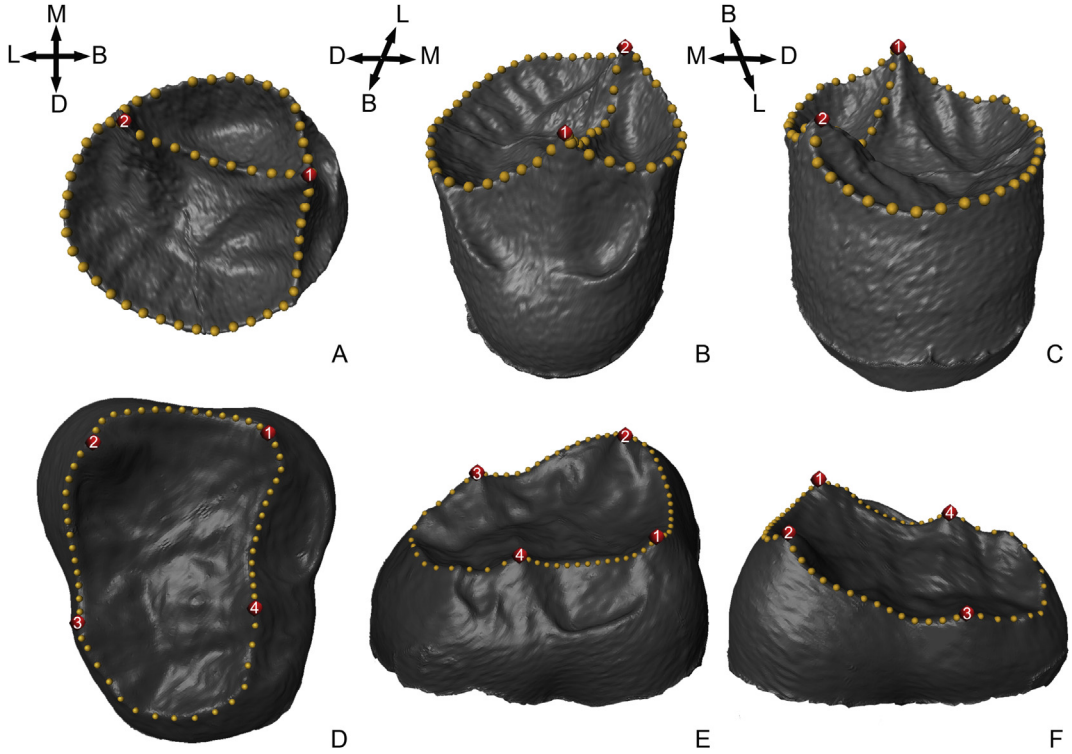

Figure 1. EDJ surface model of a lower premolar (A–C, occlusal, buccal, and lingual views of SKX 21204 from Swartkrans) and a lower molar (D–F, occlusal, buccal, and lingual views of SKW 5 from Swartkrans), illustrating the landmarks collected on the tips of the dentine horns (larger, red circles) and semi-landmarks that run between the dentine horns (yellow circles) used to capture EDJ shape. Abbreviations: buccal = B, distal = D, lingual = L, and mesial = M. See text for explanations of numbers on the red circles. Note that premolars and molars are not illustrated to scale. (For interpretation of the references to color in this figure legend, the reader is referred to the web version of this article.)

Table 2
Mean (in mm) and relative enamel thicknesses (3D AET and 3D RET) values in each taxon.

Taxon		P_3	Min-Max	P_4	Min-Max	M_1	Min-Max	M_2	Min-Max	M_3	Min-Max
P. robustus	3D AET	1.92	1.79–2.06	1.74	1.70–1.79	1.90	1.67–2.13	2.20	1.88–2.70	2.00	1.66–2.59
	3D RET	34.79	34.12–35.46	24.94	23.38–26.50	23.93	19.32–28.55	26.77	22.63–38.00	23.42	19.38–33.07
Early *Homo*	3D AET	1.48	–	1.79	–	1.77	–	–	–	1.38	–
	3D RET	29.03	–	32.97	–	27.52	–	–	–	20.05	–
Au. africanus	3D AET	–	–	1.35	–	–	–	1.83	–	1.81	–
	3D RET	–	–	22.38	–	–	–	25.74	–	28.08	–
Extant humans	3D AET	0.99	0.81–1.17	1.11	0.97–1.37	1.31	1.11–1.47	1.42	1.06–1.92	1.38	1.20–1.47
	3D RET	24.65	19.67–28.39	26.74	24.25–30.98	21.36	17.56–23.88	26.56	21.91–39.00	22.06	20.52–23.74
Neanderthals	3D AET	–	–	–	–	1.23	1.10–1.43	1.28	1.20–1.33	1.38	1.24–1.54
	3D RET	–	–	–	–	17.73	16.05–20.36	17.20	16.26–18.71	21.24	19.11–23.73

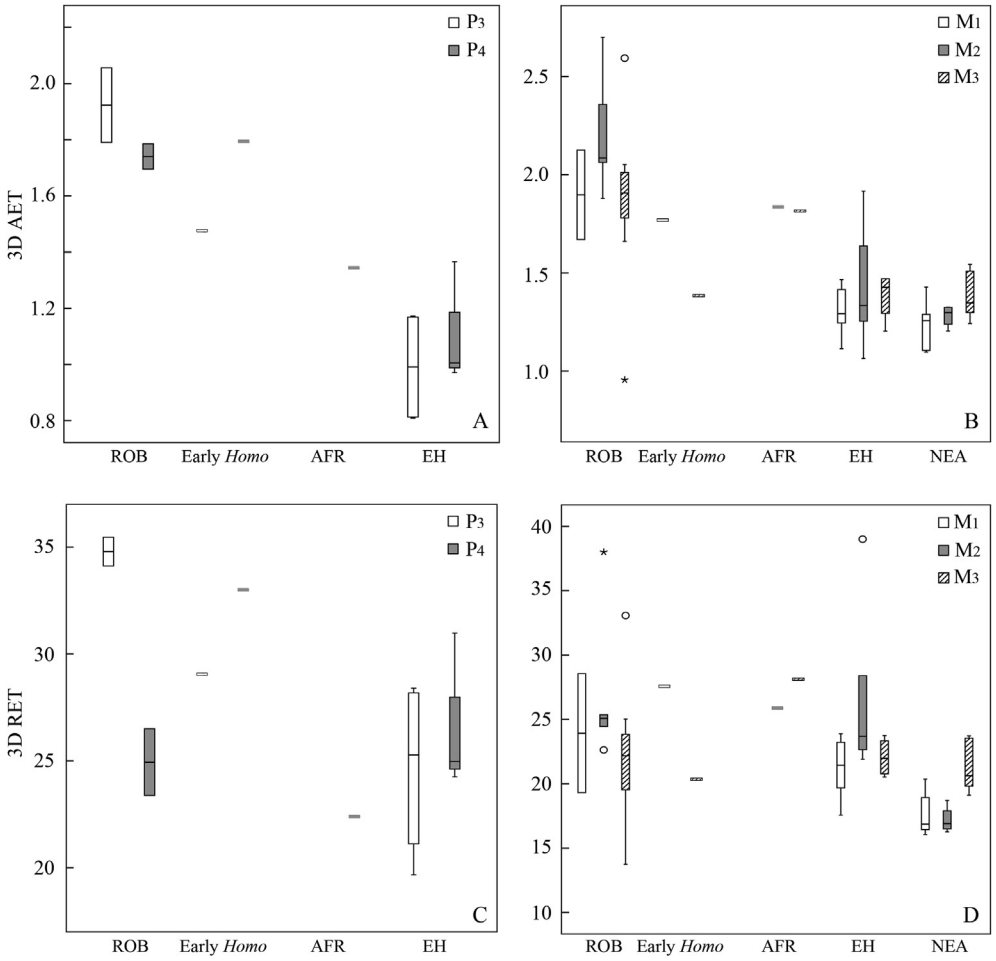

Figure 2. Average (in mm) and relative enamel thickness (3D AET and 3D RET) values in each taxon. A, B) 3D AET, C, D) 3D RET. Standard box and whisker plot reveals the interquartile range (25th–75th percentiles: boxes), 1.5 interquartile range (whiskers), and the median values (black line). Outliers more than 1.5 interquartile range from the box are signified with circles, extremes more than 3 interquartile ranges from the box are signified with asterisks. ROB = *P. robustus*, AFR = *Au. Africanus*, EH = Extant human, NEA = Neanderthals.

thicker enamel over the top or on the apex of the cusp (e.g., Figs. 3A, E and 4A). Early *Homo* show features similar to extant humans and Neanderthals, with thicker enamel on the lateral aspects of the cusps or on the lateral wall of the crown (e.g., Figs. 3B and 4B).

In *P. robustus*, the thickest part of the crown is on the apices of the cusp tips (Figs. 3A, 4A, and 6A). Thicker enamel is largely seen on the buccal and distal cusp tips rather than on the lingual cusps, but exceptions to this include SK 23 and SK 855 (SOM Fig. 4B and D). Occasionally, thicker enamel is also observed on the molar occlusal basin, where accessory cuspulids are located (Figs. 4A and 5A, B).

The enamel thickness distribution of our two *Au. africanus* individuals resembles the *P. robustus* condition. The Sts 18 LP_4 shows thicker enamel on the protoconid cusp tip, and LM_1—although it shows occlusal wear and, therefore, is not suitable for enamel thickness studies—exhibits thicker enamel on the buccal and distal wall of the crown (Figs. 3E and 4C). The other *Au. africanus* individual, Sts 52, shows thicker enamel on hypoconid and hypoconulid cusp tips and the buccal wall of the crown (Figs. 5C and 6B). Unlike *P. robustus*, our *Au. africanus* sample shows a more unbalanced expression of enamel distribution between buccal and lingual parts of the crown; thicker enamel is located on the buccal aspects,

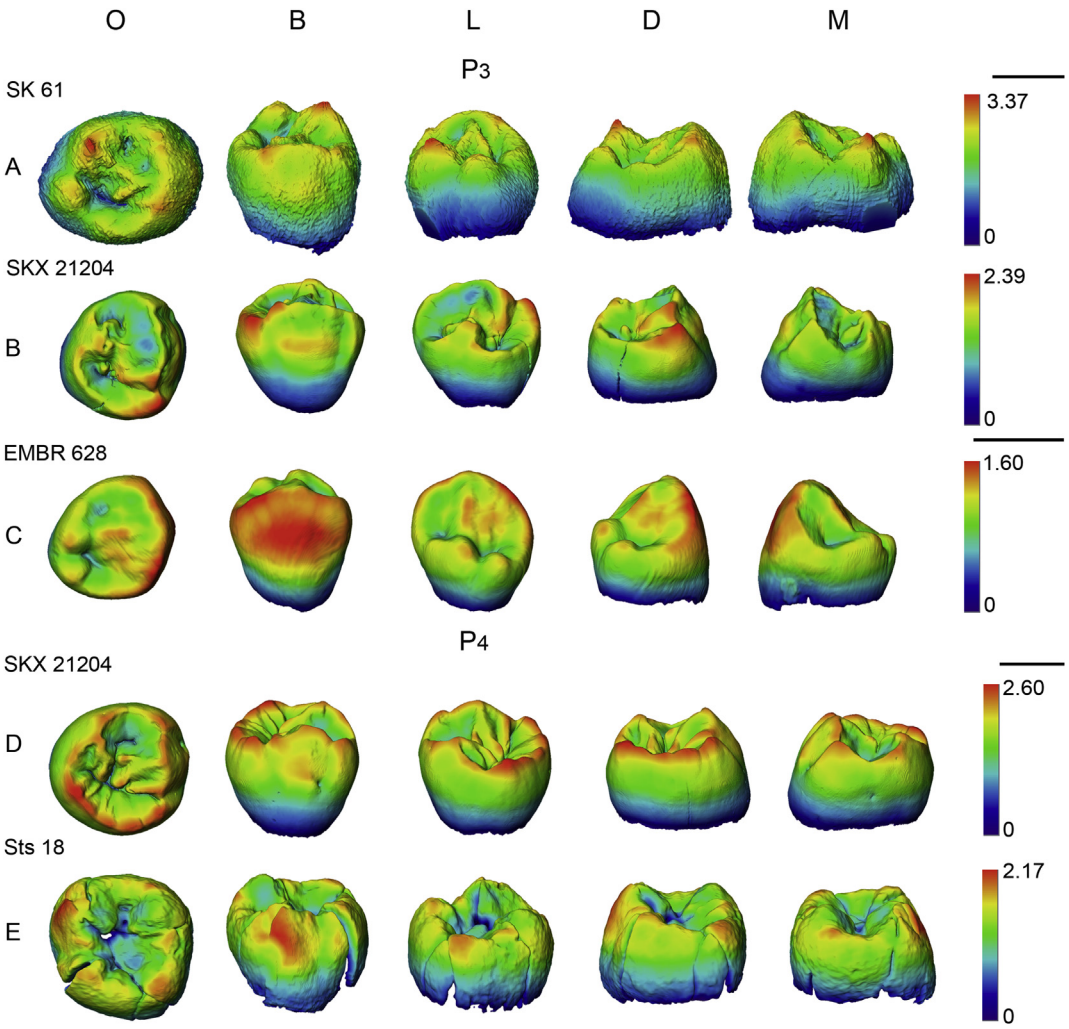

Figure 3. Enamel thickness distribution in premolars. Color scales of enamel thickness are specific to each tooth. See Figure 1 for explanations of abbreviations. Bar = 5 mm.

comparable to only a few *P. robustus* specimens such as TM 1517 and SK 843 (SOM Fig. 4C, E). It is worth noting that the remains of a cingulum are observed on the protoconid of Sts 52 M_3, forming a bridge that runs vertically on the buccal surface of the protoconid with thicker enamel on the top (Fig. 6B).

Our sample comprises only two early *Homo* premolars from a single individual (SKX 21204). The thickest enamel of P_3 is observed on the buccal end of the distal marginal ridge, which forms a small accessory cuspulid, on the buccal wall of the protoconid, between the vertical furrows near the mesial and distal crown edges, and also on the notably reduced metaconid tip (Fig. 3B). The thickest enamel of P_4 is observed along the occlusal edges of the distal marginal ridge and at a small accessory cuspulid located on the buccal end of the mesial marginal ridge (Fig. 3D). Our early *Homo* molar, SKX 257, shows a similar pattern of enamel distribution to early *Homo* premolars. Thicker enamel is observed at the distal occlusal edges of the protoconid and the hypoconulid cusp tips (Fig. 4B). Thicker enamel is also seen at the tip of a pseudocentroconid located on the occlusal basin, as shown in some *P. robustus*, modern humans, and Neanderthals (Fig. 4A, E and SOM Figs. 2A and 4I, L). In another early *Homo* specimen, SK 15 M_3, the cusps are almost worn flat, retaining little information about enamel distribution, but the lateral aspect is well preserved; the buccal wall shows much thicker enamel than the lingual wall (Fig. 6C).

The enamel thickness distribution in our extant human and Neanderthal sample shows closer affinity to early *Homo*. Thicker enamel on extant human premolars is found at the buccal wall of the protoconid (Fig. 3C and SOM Fig. 1D–E) and also along the occlusal edges of the protoconid (Fig. 3C and SOM Fig. 1G and I). In molars, thicker enamel is commonly found at the lateral wall of the buccal cusps (Figs. 4E and 5E and SOM Fig. 2B–E) and on the occlusal edges of the buccal and distal cusps (Figs. 4F and 5D and SOM Fig. 2E and F).

3.2. EDJ geometric morphometric analyses

The Neanderthal sample showed high inter-individual variation in EDJ morphology, which reduced between-group variance among other groups. We thus conducted two separate sets of analyses, one with Neanderthals and one without. Results of the multivariate analysis including the Neanderthal sample are given in SOM Figure 5 and are discussed only when we generalize to the genus *Homo*.

The results of bgPCA are shown in Figures 7–9 and SOM Figure 5. Among premolars, early *Homo* EDJ shape is separated clearly from australopiths along bgPC1. The SKX 21204 P_3 is placed within the extant human scatter (Fig. 7A), and the P_4 lies in the middle of the plot (Fig. 7B). In contrast, the molar EDJ shapes of

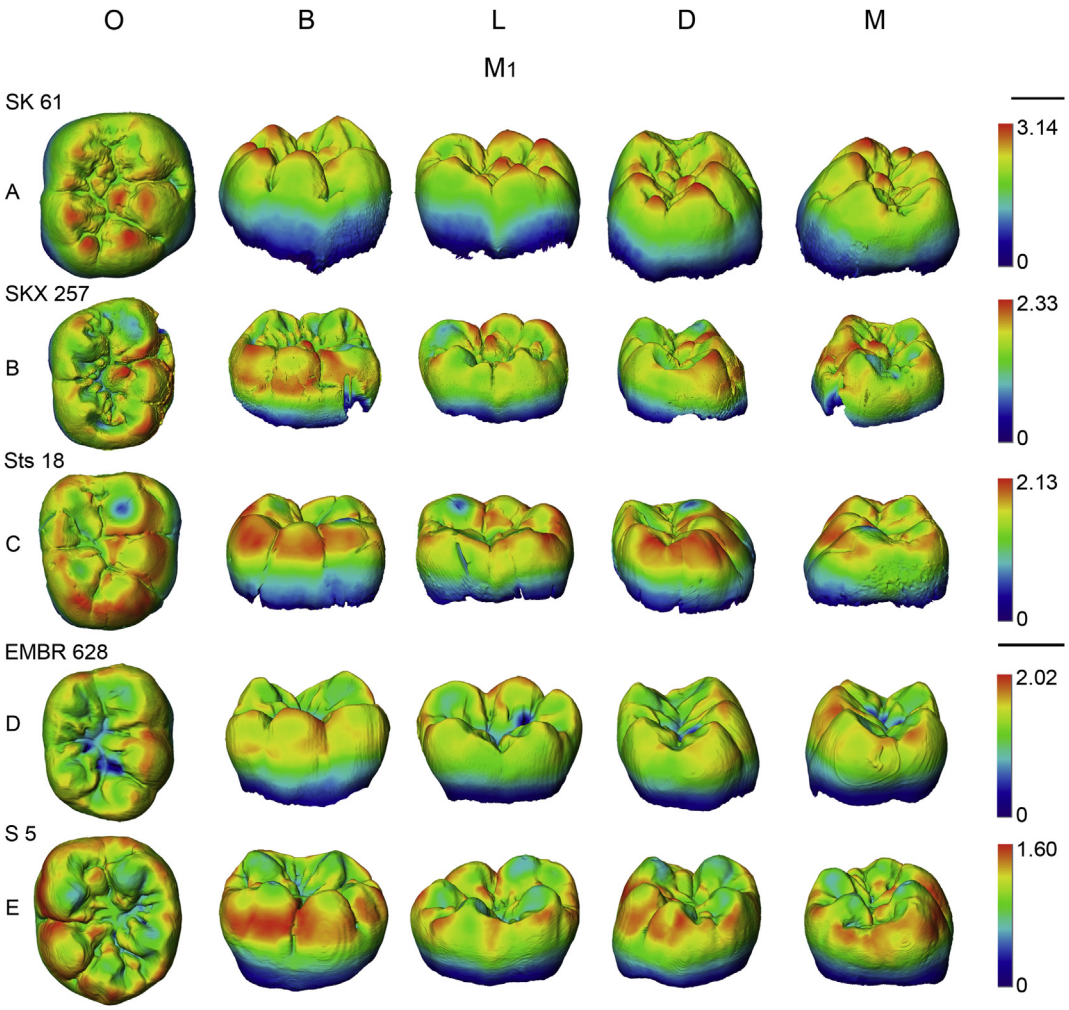

Figure 4. Enamel thickness distribution in M_1s. Color scales of enamel thickness are specific to each tooth. See Figure 1 for explanations of abbreviations. Bar = 5 mm.

early *Homo* suggest much closer affinity to *P. robustus* along bgPC1 (Fig. 8A–C). *Australopithecus* and *Paranthropus* P_3s are separated from each other along bgPC2 (Fig. 7A), but their P_4s cluster closely (Fig. 7B).

Along bgPC1, the early *Homo* and modern human P_3 is characterized by equally sized foveae anterior and posterior, an oval-shaped EDJ outline, and an elevated protoconid dentine horn (Fig. 7A, a, b). Not surprisingly, *P. robustus* premolars show a larger fovea posterior and a more trapezoidal EDJ outline, and the main cusps are placed more centrally (Fig. 7A, B, a, e). The P_3 of *Au. africanus* (Sts 52) exhibits no special affinity to any other specimens: it is placed at the upper end of bgPC2 (Fig. 7A), with a slender rectangular EDJ outline and an elevated protoconid dentine horn (Fig. 7d). In contrast, the P_4s of *P. robustus* and *Au. africanus* cluster very close to each other, and *P. robustus* shows a highly variable EDJ shape along bgPC2 (Fig. 7B). The early *Homo* P_4 shows a mix of australopith and modern human features, with no particular assocciation to other groups. Landmarks with the highest eigenvalues are commonly found at either side of the dentine horn tips, suggesting that the area around dentine horn tips contributes most to shape variation (Fig. 7C).

For molars, *Au. africanus* is located at the zero point of bgPC1, which separates early *Homo* from extant humans. *Australopithecus africanus* is separate from other groups on bgPC2 (Fig. 8A–C). In all cases, the three *Homo* groups are scattered, showing few signs of clustering (SOM Fig. 5A–C). In both bgPCs, early *Homo* molars plot close to *P. robustus*, being placed at the lower end of bgPC1, while modern humans cluster at the upper end. The early *Homo* molars have a consistent, rectangular EDJ outline. Compared with modern humans, the early *Homo* and *P. robustus* EDJ is characterized by a flattened topology, with lower and centrally placed dentine horns, and a mesiodistally elongated outline (Figs. 8A–C and 9A–G). It is worth noting that SK 15, our early *Homo* M_2, falls just outside the *P. robustus* sample, characterized by an oval-rectangular outline and distally expanded marginal ridge, when compared to extant humans (Figs. 8B and 9E). Moreover, the hypoconulid dentine horns are barely visible in extant human M_2s, but are pronounced in fossil hominins (Fig. 9F). With regeard to M_3s, early *Homo* again lies at the zero point of the plot, but unlike P_4, our early *Homo* M_3 is placed within the *P. robustus* range (Fig. 8C).

Australopithecus africanus molars consistently show features transitional from fossil hominins to extant humans along bgPC1. Along bgPC2, the *Au. africanus* M_1 shows lower lingual dentine horns (Fig. 9D), M_2 and M_3 are characterized by centrally placed metaconid dentine horns (Fig. 9G, K), and M_2 also shows a pronounced hypoconulid dentine horn (Fig. 9H). In addition, *Au. africanus* molars can be distinguished on the basis of their EDJ outlines; M_1 shows a buccolingually narrow outline and M_2–M_3 show ovo rectangular outlines (Fig. 8A–C). As already noted, *Au. africanus* molars have slightly more elevated dentine horns than *P. robustus*

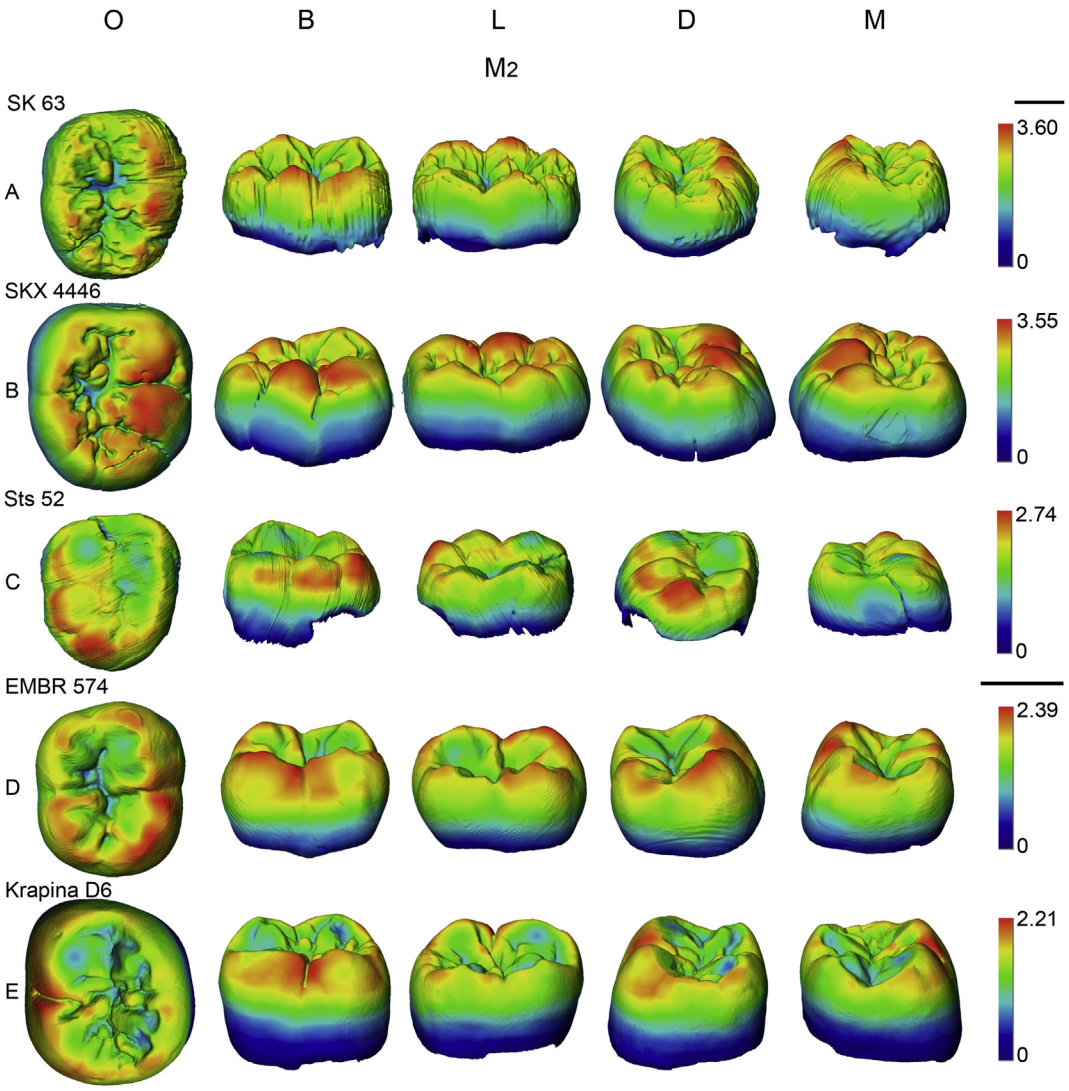

Figure 5. Enamel thickness distribution in M_2s. Color scales of enamel thickness are specific to each tooth. See Figure 1 for explanations of abbreviations. Bar = 5 mm.

(Skinner et al., 2008b). This is consistent with our results, as bgPC1 probably contributes to variation of dentine horn height, although our study has a small sample size. Like in the premolars, landmarks with the highest eigenvalues are commonly placed at either side of the dentine horn tips, at the lowest point of ridge curves that connect two dentine horns (Fig. 8D).

When the Neanderthal sample is included in analysis, Neanderthals and modern humans form two separate groups along bgPC2 (SOM Fig. 5A–C), and Neanderthal M_1s and M_3s show appreciable inter-individual variation, with the distribution covering one-half of the axis/plot (e.g., SOM Fig. 5A and C). It is also interesting to note that when we introduce Neanderthal data, the M_1 of *Au. africanus* plots with modern humans, which is probably due to the strongly centrally placed lingual dentine horns in the Neanderthal sample, a distinct character that "compresses" between-group dispersion (SOM Fig. 5A–C, c, g, k). Neanderthals also show high protoconid dentine horns, and M_3s show an excessively deep and curved mesial marginal ridge. The shape differences among other species are unclear in the plot for there is a significant inter-individual variation in Neanderthals, although the sample size is small and our generalization is based on landmark shapes yielded by GPA and bgPCA, at either end of the axes (SOM Fig. 5k). However, it is clear that early *Homo* molars have a closer similarity to *P. robustus* than to other *Homo* groups.

4. Discussion

4.1. Variation in enamel thickness parameters and distribution between groups

We observe a trend for an increase in 3D AET and RET along the premolar dentition in the modern human group and our early *Homo* individual. However, a limited sample size currently prevents statistical generalization of early *Homo* enamel thickness. No clear relationship is found between 3D enamel thickness and molar position in australopiths, as already suggested by other studies (Olejniczak et al., 2008b). We also find that extant human premolars have significantly thinner RET than *P. robustus* (SOM Table 3). Our results on 3D molar enamel thickness in extant humans are consistent with cross-sectional studies. They indicate that extant human M_1s have significantly thinner enamel than M_2s and M_3s (Grine, 2005; Smith et al., 2005). It is unclear if early *Homo* also shows this trend, as owing to a small sample size and occlusal

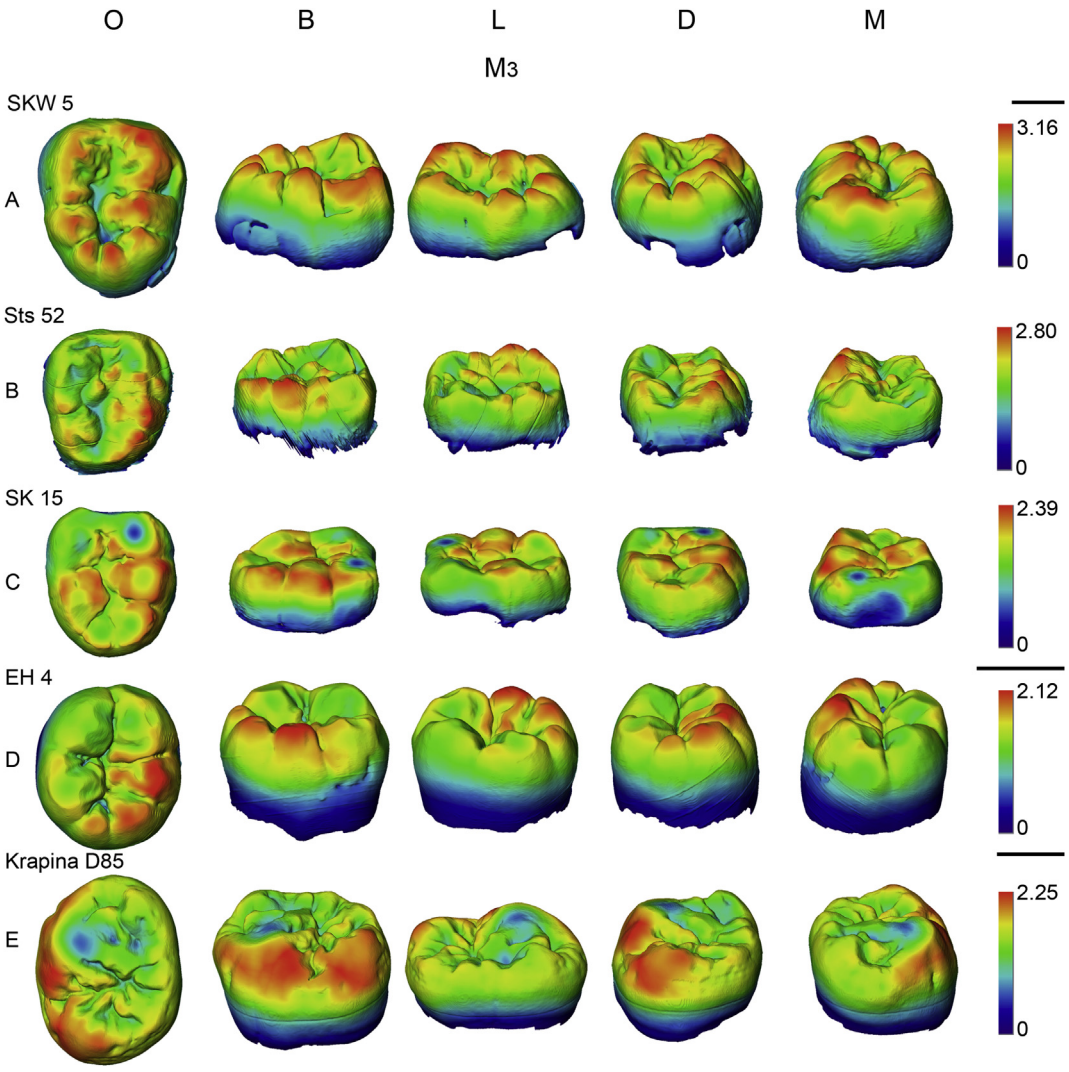

Figure 6. Enamel thickness distribution in M_3s. Color scales of enamel thickness are specific to each tooth. See Figure 1 for explanations of abbreviations. Bar = 5 mm.

wear in SK 15, general comparisons of enamel thickness between molar positions in early *Homo* are not available.

Based on the relative enamel thickness categories developed by Martin (1985) and Grine and Martin (1988), we found that *P. robustus* and early *Homo* have similar thick to hyper thick premolars, while *Au. africanus* and extant humans have thick premolars. Early *Homo* molars show thick enamel exceeding or lying within respective modern human values (even though our early *Homo* M_3 has a degree of wear, its enamel thickness is the minimum estimation), and 2D measurements yielded the same results (Smith et al., 2012). Our 3D reconstructions showing thick-enameled molars in *Au. africanus* are similar to the conclusions reached from cross-sectional 2D measurements (Grine and Martin, 1988; Olejniczak et al., 2008b; Skinner et al., 2015). Our results are different from another study using 3D measurements, which suggests that *Au. africanus* molars have moderately thick enamel (Olejniczak et al., 2008b). Our *P. robustus* molar RET data are consistent with those from other 2D and 3D studies, suggesting it is thick but not hyper thick (Olejniczak et al., 2008b; Skinner et al., 2015). Our data on Neanderthal molar enamel thickness are consistent with a number of micro-tomographic analyses (Macchiarelli et al., 2006; Olejniczak et al., 2008a; Benazzi et al., 2011a, 2015).

It is believed that relatively thick molar enamel in recent humans (probably linked to a prolonged lifespan and ontogenetic period) is achieved through a different developmental mechanism than in early thick-enameled hominins (including australopiths and *H. erectus*; Dean et al., 2001). Indeed, thick molar enamel in modern humans is the result of a unique odontogenetic process (a reduction of tooth size by decreasing the quantity of the coronal dentine, instead of functional/adaptive mechanisms; Grine, 2002, 2005), and therefore has a limited value for hominin taxonomy (Smith et al., 2012; Skinner et al., 2015). However, it is believed that such developmental loss of coronal dentine and molar crown size is not present in Neanderthals, as Neanderthal molars comprise less enamel and more dentine than those of extant humans (Olejniczak et al., 2008a). In addition, Neanderthals show a more complex EDJ surface, with about 10% greater area than modern humans (Macchiarelli et al., 2006), resulting in thinner enamel thickness.

Schwartz (2000) noted that the distribution of enamel thickness could be a strong taxonomic and functional indicator. The relationship between molar enamel distribution and dietary adaptation has been explored subsequently with 2D and 3D methods, indicating that tooth functions may be better understood in terms of 3D distribution of crown enamel, rather than from

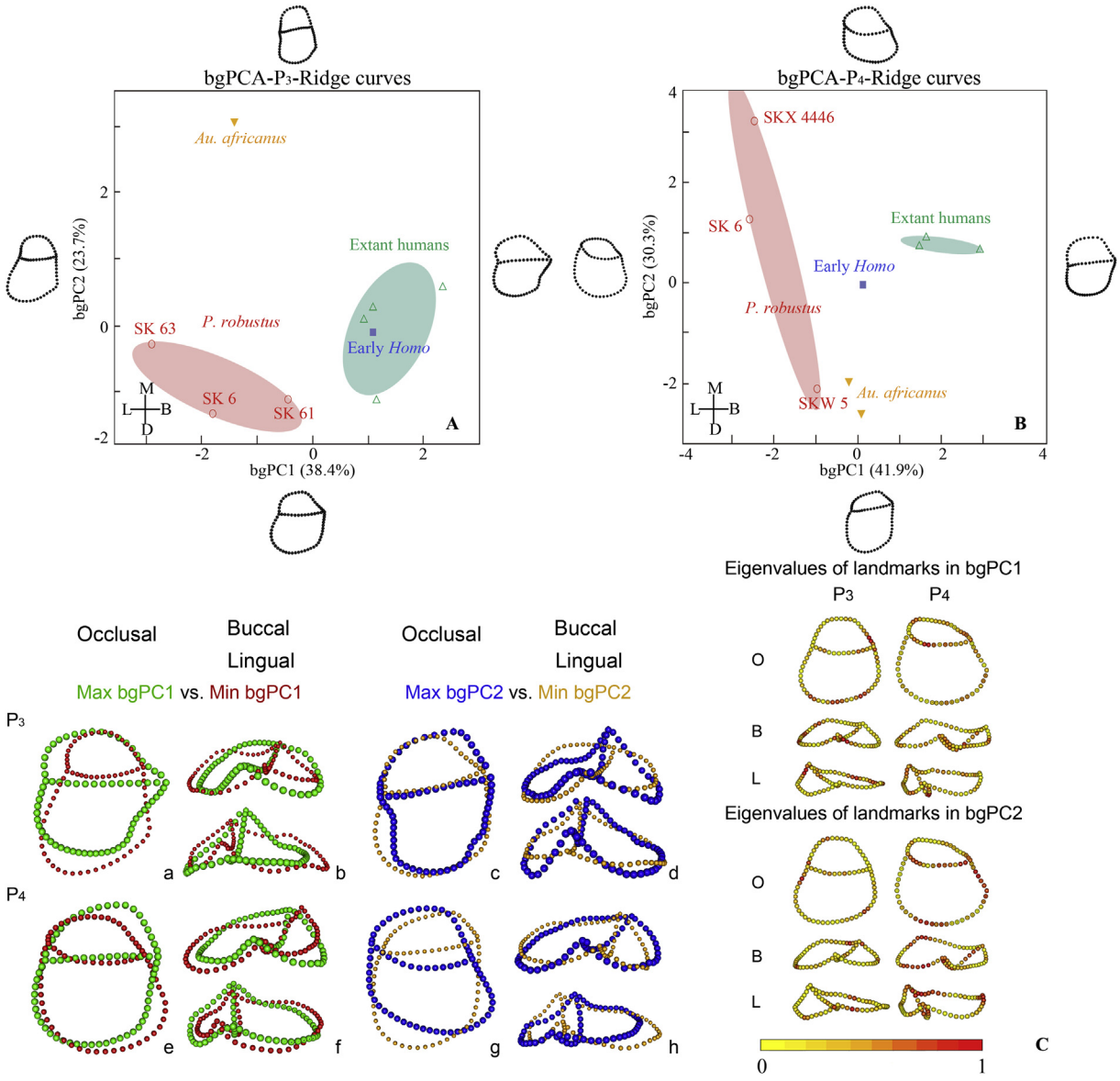

Figure 7. A, B) Results of bgPCAs of the semi-landmark configurations of P_3 and P_4, respectively. BgPC1 and bgPC2 represent components of the shape variation, the 95% confidence ellipses are presented, and ridge curves shown at the end of each axis illustrate the conformation trends of shape along each PC. C) Eigenvalues of each landmark involved in bgPCAs. The range of the eigenvalues is from −1 to 1. The bar denotes absolute values of the eigenvalues. See Figure 1 for explanations of abbreviations. a—h) Landmark series of EDJ after Procrustes superimposition and bgPCA. (The reader is referred to the web version of this article for colored figures.)

enamel thickness indices extracted from a single section plane (Macho and Thackeray, 1993; Kono et al., 2002; Kono, 2004; Kono and Suwa, 2008; Olejniczak et al., 2008b; Suwa et al., 2009; Skinner et al., 2015). The early *Homo* molars sampled in this study share a similar distribution pattern with *H. erectus* and extant *H. sapiens*, where the thickest enamel is commonly found at lateral aspects of a cusp, around cusp bases, and at the buccal aspect of the hypoconulid, rather than the occlusal aspect of the crown (Grine, 2005; Olejniczak et al., 2008b; Zanolli, 2015). We also observe thicker enamel along or at the end of marginal ridges and crests in *Homo* specimens, together with proportionately thicker enamel on the lateral surfaces of the "functional" cusps. This may prolong functional crown life by dispersing masticatory forces and by preventing cusp fracture, rather than being an adaptation to hard/abrasive object feeding (Macho and Spears, 1999; Grine, 2005). Moreover, studies on dental biomechanics in human molars suggest marginal ridges might be high stress-bearing areas (Benazzi et al., 2013), indicating that our observed differences in enamel distribution along marginal ridges between *Homo* and australopiths could reflect differences in food processing. As has been suggested, occlusal topography, like the presence of grooves, crests, and cusp sharpness, might have more important biomechanical implications than enamel thickness (Benazzi et al., 2013; Berthaume, 2014; Berthaume et al., 2014). Similar enamel thickness distribution patterns among our early and later members of the genus *Homo* suggest that this dietary or functional adaptation has probably emerged along the origin of the *Homo* lineage. On the other hand, thick cuspal enamel exhibited along the postcanine dentition of australopiths could be an adaptation to increase the attritional longevity of wear facets in response to abrasive diet (Lucas et al., 2008). Studies on enamel thickness in other mammals such as cave bears also support that thick enamel could be considered as an adaptation to hard and abrasive plant-based food sources, while thin enamel could indicate an

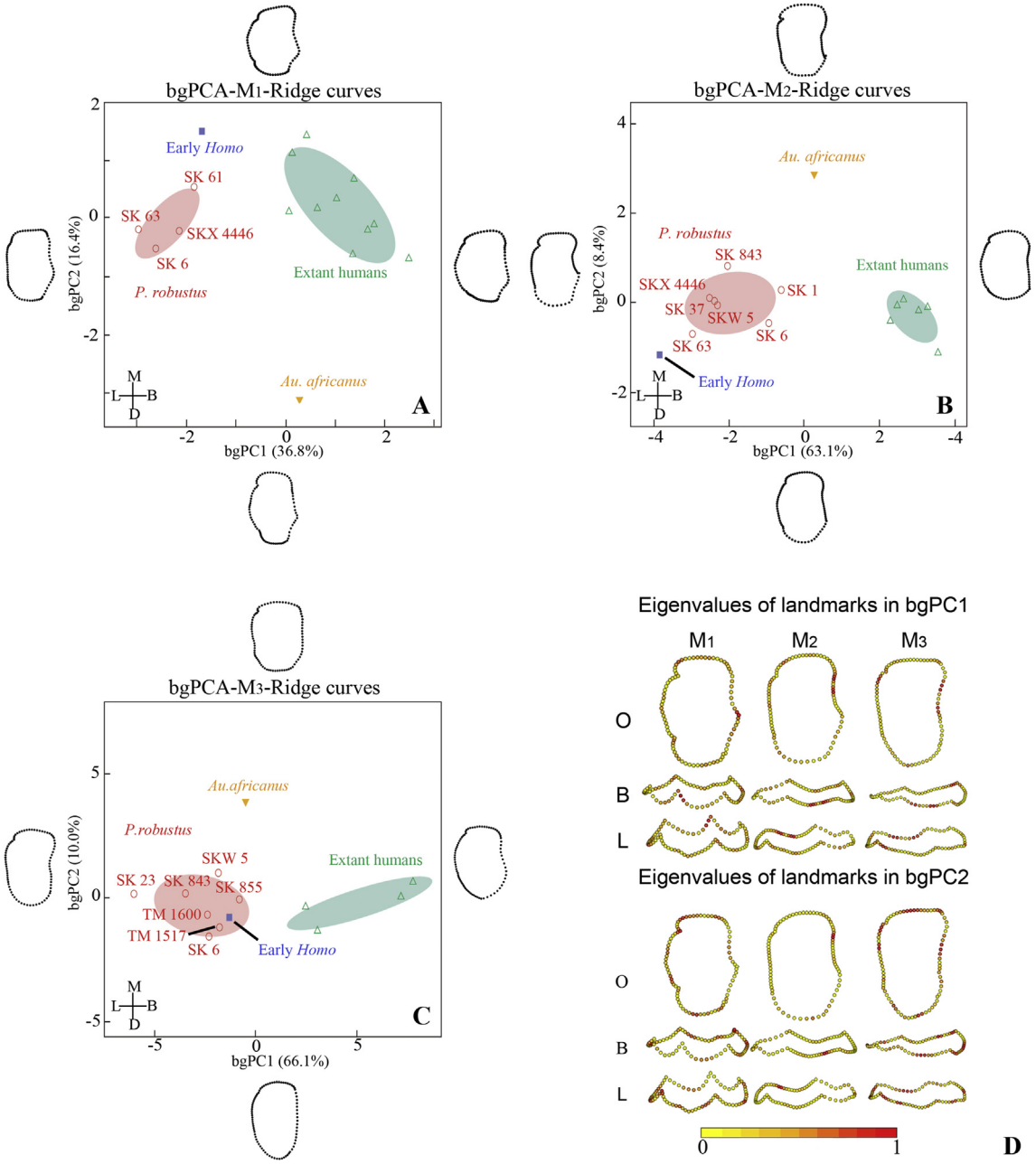

Figure 8. A–C) Results of bgPCAs of the semi-landmark configurations of M_1–M_3, respectively. BgPC1 and bgPC2 represent components of the shape variation, the 95% confidence ellipses are presented, and ridge curves shown at the end of each axis illustrate the conformation trends of shape along each PC. D) Eigenvalues of each landmark involved in bgPCAs. The range of the eigenvalues is from −1 to 1. The bar denotes absolute values of the eigenvalues. See Figure 1 for explanations of abbreviations.

exclusive carnivorous diet (Mackiewicz et al., 2010). Our data on enamel thickness distribution are in line with previous studies demonstrating diversified dietary habits between *P. robustus* and early *Homo*, and the more specialized masticatory apparatus of *P. robustus* (Laden and Wrangham, 2005; Balter et al., 2012). As stated by Villmoare et al. (2015), genus *Homo* may arise at ca. 2.8 Ma (but see Hawks et al., 2015), and further investigations of enamel thickness distribution in early *Homo* species in East Africa may yield a better understanding of the evolutionary trends and adaptive significance of enamel thickness distribution in early *Homo*. Our database on enamel thickness and its distribution pattern could offer some insights into the affinity of specific taxonomically uncertain specimens.

4.2. Variation in EDJ morphology between groups

The differences we observe between *P. robustus* and *Au. africanus* molars in dentine horn height, relative dentine horn positions, and EDJ outline have already been reported (Robinson, 1956; Suwa et al., 1996; Olejniczak et al., 2008a; Skinner et al., 2008b). However, we record a transitional feature on the EDJ level, along the postcanine dentition of our early *Homo* sample. In particular, premolars of early *Homo* show EDJ shapes that closely approximate the extant human condition, with equal-sized foveae anterior and posterior, and higher protoconid dentine horns, while the molars show a relatively low EDJ topography associated with a mesiodistally elongated occlusal basin, to some extent reminiscent

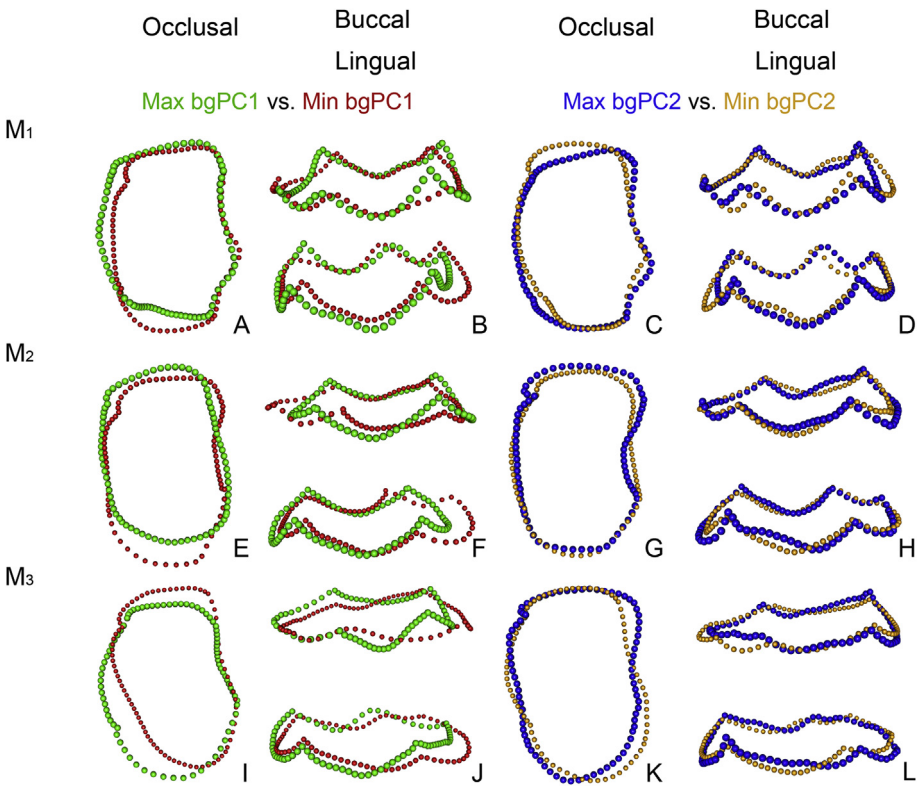

Figure 9. Landmark series of EDJ after Procrustes superimposition and bgPCA. (The reader is referred to the web version of this article for colored figures.)

of the primitive hominin condition (Macchiarelli et al., 2004; Skinner et al., 2008b; Braga et al., 2010). Similar primitive features are also evident on the lower molars of some African *H. erectus/ergaster* and *Homo heidelbergensis*, while Javanese *H. erectus* displays derived morphology approximating that seen in modern humans (Zanolli et al., 2014; Zanolli, 2015). As shown by other studies, molar EDJ shape is somewhat taxonomically informative among hominins (e.g., Corruccini, 1987; Skinner et al., 2008b). However, while the premolars of South African early *Homo* show closer affinities to extant humans, their molars certainly cluster with those of australopiths. Moreover, while the upper second molar EDJ of early *Homo* can be distinguished well from australopiths (Fornai et al., 2015), we found the lower molars to be much closer to the australopith condition. Our bgPCA shows higher eigenvalues at either side of the dentine horn tips, and also at the lowest point of the marginal ridge, and different parts of the marginal ridges show different degrees of contribution to shape variation; this may suggest the position of dentine horn tips alone is a relatively weak indicator to shape variation.

A study on molar GM in capuchins suggests that molar shapes reflect different influences depending on molar position (i.e., M_1 represents phylogenetic affinities and M_2 indicates biogeographic variability; Delgado et al., 2015), probably due to differences in biomechanical demands and the magnitude of biting forces involved in food processing (Spencer, 2003). Our observed differential expression of EDJ morphology in hominin postcanine dentition related to tooth position could also, therefore, represent different influences.

A previous study on the biomechanical implications of EDJ topography suggests that the grooves, fissures, and crests might act to increase the structural stiffness of the tooth, as they are the stress-bearing features (Benazzi et al., 2011b). This supports the hypothesis that a strong expression of the protostylid in *Au. africanus* molar EDJ could reinforce the crown, a suggested dietary adaptation (Skinner et al., 2009). Previous studies also correlated enamel thickness, EDJ shape, and diet (Martin, 1983; Macchiarelli et al., 2006; Suwa et al., 2007; El Zaatari et al., 2011), but enamel thickness and EDJ shape are not necessarily connected (Smith et al., 2006). Relatively tall dentine horn tips might be associated with thin enamel in *Gorilla* molars, as both characters are related to folivory (Martin, 1983), while a relatively flat dentine horn tip and thick enamel suggest a concurrent adaptation to hard and/or abrasive food items (Suwa et al., 2007). Thin enamel and complex EDJ topography in Neanderthals compared to modern humans (Macchiarelli et al., 2006) could indicate a high proportion of meat in the diets of Neanderthals (El Zaatari et al., 2011). We suggest that the thick enamel and higher/lower dentine horns in *Au. africanus*/*P. robustus* could, therefore, represent dietary diversification. Nevertheless, further studies on paleodiet, biomechanics, and EDJ surface complexity are needed.

5. Conclusion

Analyses of mandibular postcanine 3D enamel thickness reveal considerable overlap among the *P. robustus*, *Au. africanus*, South African early *Homo,* and extant humans. While we observed significant differences in enamel thickness between australopiths and extant humans, all four taxa investigated here show relatively thick enamel. This result supports the idea that measures of enamel thickness have limited taxonomic value in hominins, although the relatively thinner molar enamel in Neanderthals compared with modern humans is still a valid taxonomic indicator.

Whole-crown enamel thickness distribution patterns may yield important evidence for dietary adaptation. We conclude that

thicker enamel is observed at the lateral aspects of cusps and crown in modern humans and some fossil *Homo* (Grine, 2005; Olejniczak et al., 2008b; Zanolli et al., 2014), and was present in some of the earliest members of the genus *Homo*, suggesting occupation of a different dietary niche as compared to South African australopiths. However, as our data on whole-crown enamel distribution are restricted to qualitative description, without statistical evaluation, interpretations based on whole-crown enamel distribution should be made with caution.

High resolution micro-CT imaging coupled with 3D geometric morphometric analyses of the EDJ can be useful for taxonomic comparisons. While mosaic features are evident throughout the history of human evolution, especially in transitional species (e.g., Kivell et al., 2011; Villmoare et al., 2015), it is not surprising that we observed a mix of australopith (flattened and elongated EDJ morphology) and *Homo*-like (premolar EDJ morphology) characters in our South African early *Homo* sample. However, given the lack of early *Homo* specimens, the evolutionary/adaptive significance of different EDJ morphologies in the postcanine dentition of early *Homo*, australopiths, and extant humans is still unclear. The recent discovery of *Homo naledi* enriches the *Homo* fossil record (Berger et al., 2015). While we observed a complex occlusal surface in our unworn early *Homo* specimens, *H. naledi* lower postcanine dentition shows a complex occlusal surface in premolars, but a rather simple topography in molars. A comparative study of dental inner structure of *H. naledi* will further improve our understanding of the evolution of genus *Homo* in South Africa. Our results indicate that premolar EDJ morphology has more discriminatory power when distinguishing genus *Homo* (including Neanderthal) from australopiths. While most studies of EDJ morphology are focused on molars, few investigations have established variation in premolar EDJ morphology, and its contribution to understanding taxonomy needs to be examined with other Plio-Pleistocene hominin species.

The fossil record of South African early *Homo* dentition is rather limited, but in the meantime, it appears that some taxonomically distinctive features evident in the premolars of extant humans were already present in the early members of the genus *Homo*, and molar EDJ shapes are highly variable within the genus *Homo*. Comparative studies on the East African *H. habilis* and *H. erectus* would shed light on the evolutionary dynamics of EDJ morphology in early members of the genus *Homo*.

Acknowledgments

This work was supported by the Centre National de la Recherche Scientifique, the French Ministry of Foreign Affairs, the French Embassy in South Africa through the Cultural and Cooperation Services, and the China Scholarship Council. We thank Stephany Potze, curator of the Palaeontology Section of the Ditsong National Museum of Natural History (Pretoria), for her continuous support. We appreciate Professor Roberto Macchiarelli for his valuable insights on the Neanderthal taxonomy and chronology. We thank Dr. A. Beaudet for her technical support during the image processing of data and the statistical analysis. We are also indebted to Dr. C. Zanolli for providing CT data of extant human and Neanderthal specimens. We thank N. Ngoloyi for proofreading. We thank three anonymous reviewers and the Associated Editor for their valuable comments which helped us to improve the manuscript.

Supplementary Online Material

Supplementary online material related to this article can be found at http://dx.doi.org/10.1016/j.jhevol.2016.05.003.

References

Bailey, S.E., Benazzi, S., Souday, C., Astorino, C., Paul, K., Hublin, J.-J., 2014. Taxonomic differences in deciduous upper second molar crown outlines of *Homo sapiens*, *Homo neanderthalensis* and *Homo erectus*. J. Hum. Evol. 72, 1–9.
Balter, V., Blichert-Toftv, J., Braga, J., Telouk, P., Thackeray, F., Albarède, F., 2008. U-Pb dating of fossil enamel from the Swartkrans Pleistocene hominid site, South Africa. Earth Planet. Sci. Lett. 267, 236–246.
Balter, V., Braga, J., Télouk, P., Thackeray, J.F., 2012. Evidence for dietary change but not landscape use in South African early hominins. Nature 489, 558–560.
Benazzi, S., Fornai, C., Bayle, P., Coquerelle, M., Kullmer, O., Mallegni, F., Weber, G.W., 2011a. Comparison of dental measurement systems for taxonomic assignment of Neanderthal and modern human lower second deciduous molars. J. Hum. Evol. 61, 320–326.
Benazzi, S., Kullmer, O., Grosse, I.R., Weber, G.W., 2011b. Using occlusal wear information and finite element analysis to investigate stress distributions in human molars. J. Anat. 219, 259–272.
Benazzi, S., Nguyen, H.N., Kullmer, O., Hublin, J.-J., 2013. Unravelling the functional biomechanics of dental features and tooth wear. PLoS One 8, e69990.
Benazzi, S., Panetta, D., Fornai, C., Toussaint, M., Gruppioni, G., Hublin, J.-J., 2014. Technical Note: Guidelines for the digital computation of 2D and 3D enamel thickness in hominoid teeth. Am. J. Phys. Anthropol. 153, 305–313.
Benazzi, S., Slon, V., Talamo, S., Negrino, F., Peresani, M., Bailey, S.E., Sawyer, S., Panetta, D., Vicino, G., Starnini, E., 2015. The makers of the Protoaurignacian and implications for Neandertal extinction. Science 348, 793–796.
Berger, L., Hawks, J., de Ruiter, D.J., Churchill, S., Schmid, P., Delezene, L., Kivell, T., Garvin, H., Williams, S., DeSilva, J., Skinner, M., Musiba, C., Cameron, N., Holliday, T., Harcourt-Smith, W., Ackermann, R., Bastir, M., Bogin, B., Bolter, D., Brophy, J., Cofran, Z., Congdon, K., Deane, A., Dembo, M., Drapeau, M., Elliott, M., Feuerriegel, E., Garcia-Martinez, D., Green, D., Gurtov, A., Irish, J., Kruger, A., Laird, M., Marchi, D., Meyer, M., Nalla, S., Negash, E., Orr, C., Radovčić, J., Schroeder, L., Scott, J., Throckmorton, Z., Tocheri, M., VanSickle, C., Walker, C., Wei, P., Zipfel, B., 2015. *Homo naledi*, a new species of the genus *Homo* from the Dinaledi Chamber, South Africa. eLife 4, e09560.
Berger, L.R., Lacruz, R., de Ruiter, D.J., 2002. Revised age estimates of *Australopithecus*-bearing deposits at Sterkfontein, South Africa. Am. J. Phys. Anthropol. 119, 192–197.
Berthaume, M.A., 2014. Tooth cusp sharpness as a dietary correlate in great apes. Am. J. Phys. Anthropol. 153, 226–235.
Berthaume, M.A., Dumont, E.R., Godfrey, L.R., Grosse, I.R., 2014. The effects of relative food item size on optimal tooth cusp sharpness during brittle food item processing. J.R. Soc. Interface 11, 20140965.
Beynon, A., Wood, B., 1986. Variations in enamel thickness and structure in east African hominids. Am. J. Phys. Anthropol. 70, 177–193.
Beynon, A., Wood, B., 1987. Patterns and rates of enamel growth in the molar teeth of early hominids. Nature 326, 493–496.
Billy, G., Vallois, H., 1977a. La mandibule pré-Rissienne de Montmaurin. L'Anthropologie 81, 273–312.
Billy, G., Vallois, H., 1977b. La mandibule pré-Rissienne de Montmaurin (suite). L'Anthropologie 81, 411–458.
Braga, J., Thackeray, J.F., Subsol, G., Kahn, J.L., Maret, D., Treil, J., Beck, A., 2010. The enamel-dentine junction in the postcanine dentition of *Australopithecus africanus*: intra-individual metameric and antimeric variation. J. Anat. 216, 62–79.
Braga, J., Thackeray, J.F., Dumoncel, J., Descouens, D., Bruxelles, L., Loubes, J.-M., Kahn, J.-L., Stampanon, M., Bam, L., Hoffman, J., de Beer, F., Spoor, F., 2013. A new partial temporal bone of a juvenile hominin from the site of Kromdraai B (South Africa). J. Hum. Evol. 65, 447–456.
Brain, C., 1975. An interpretation of the bone assemblage from the Kromdraai australopithecine site, South Africa. In: Tuttle, R.H. (Ed.), Paleoanthropology, Morphology and Paleoecology. Walter de Gruyter, Berlin, pp. 225–243.
Brain, C., 1981. The Hunters or the Hunted? University of Chicago Press, Chicago.
Broom, R., 1938. The Pleistocene anthropoid apes of South Africa. Nature 142, 377–379.
Broom, R., 1949. Another new type of fossil ape-man. Nature 163, 57.
Broom, R., Robinson, J.T., 1949. A new type of fossil man. Nature 164, 322–323.
Broom, R., Robinson, J.T., 1952. Swartkrans ape-man, *Paranthropus crassidens*. Trans. Mus. Mem. No. 6, 1–124.
Butler, P., 1956. The ontogeny of molar pattern. Biol. Rev. 31, 30–69.
Clarke, R., 1994. On some new interpretations of Sterkfontein stratigraphy. S. Afr. J. Sci. 90, 211–214.
Corruccini, R., 1987. The dentinoenamel junction in primates. Int. J. Primatol. 8, 99–114.
Dean, C., Leakey, M.G., Reid, D., Schrenk, F., Schwartz, G.T., Stringer, C., Walker, A., 2001. Growth processes in teeth distinguish modern humans from *Homo erectus* and earlier hominins. Nature 414, 628–631.
Debénath, A., 1977. The latest finds of antéwürmian human remains in Charente (France). J. Hum. Evol. 6, 297–302.
Delgado, M.N., Galbany, J., Górka, K., Pérez-Pérez, A., 2015. Taxonomic implications of molar morphology variability in Capuchins. Int. J. Primatol. 36, 707–727.
El Zaatari, S., Grine, F., Ungar, P.S., Hublin, J.-J., 2011. Ecogeographic variation in Neandertal dietary habits: evidence from occlusal molar microwear texture analysis. J. Hum. Evol. 61, 411–424.
Fornai, C., Benazzi, S., Svoboda, J., Pap, I., Harvati, K., Weber, G.W., 2014. Enamel thickness variation of deciduous first and second upper molars in modern humans and Neanderthals. J. Hum. Evol. 83–91.

Fornai, C., Bookstein, F.L., Weber, G.W., 2015. Variability of *Australopithecus* second maxillary molars from Sterkfontein Member 4. J. Hum. Evol. 85, 181–192.
Gibbon, R.J., Pickering, T.R., Sutton, M.B., Heaton, J.L., Kuman, K., Clarke, R.J., Brain, C., Granger, D.E., 2014. Cosmogenic nuclide burial dating of hominin-bearing Pleistocene cave deposits at Swartkrans, South Africa. Quat. Geochronol. 24, 10–15.
Girard, M., 1973. La brèche à "Machairodus" de Montmaurin (Pyrénées centrales). Bulletin de l'AFEQ 3, 193–207.
Grine, F.E., 1989. New hominid fossils from the Swartkrans formation (1979–1986 excavations): craniodental specimens. Am. J. Phys. Anthropol. 79, 409–449.
Grine, F.E., Daeglin, D.J., 1993. New mandible of *Paranthropus robustus* from Member 1, Swartkrans Formation, South Africa. J. Hum. Evol. 24, 319–333.
Grine, F.E., 2002. Scaling of tooth enamel thickness, and molar crown size reduction in modern humans: research letter. S. Afr. J. Sci. 98, 503–509.
Grine, F.E., 2005. Enamel thickness of deciduous and permanent molars in modern *Homo sapiens*. Am. J. Phys. Anthropol. 126, 14–31.
Grine, F.E., Martin, L., 1988. Enamel thickness and development in *Australopithecus* and *Paranthropus*. In: Grine, F.E. (Ed.), Evolutionary history of the "robust" australopithecines. Aldine de Gruyter, New York, pp. 3–42.
Gunz, P., Ramsier, M., Kuhrig, M., Hublin, J.-J., Spoor, F., 2012. The mammalian bony labyrinth reconsidered, introducing a comprehensive geometric morphometric approach. J. Anat. 220, 529–543.
Hawks, J., de Ruiter, D.J., Berger, L.R., 2015. Comment on "Early *Homo* at 2.8 Ma from Ledi-Geraru, Afar, Ethiopia". Science 348, 1326.
Hlusko, L., 2002. Identifying metameric variation in extant hominoid and fossil hominid mandibular molars. Am. J. Phys. Anthropol. 118, 86–97.
Hoffman, J.W., de Beer, F., 2012. Characteristics of the micro-focus X-ray tomography facility (MIXRAD) at Necsa in South Africa, 18th World Conference on Nondestructive Testing, Durban, South Africa.
Kay, R., 1981. The nut-crackers—a new theory of the adaptations of the Ramapithecinae. Am. J. Phys. Anthropol. 55, 141–151.
Kay, R., 1985. Dental evidence for the diet of *Australopithecus*. A. Rev. Anthropol. 14, 315–341.
Kivell, T.L., Kibii, J.M., Churchill, S.E., Schmid, P., Berger, L.R., 2011. *Australopithecus sediba* hand demonstrates mosaic evolution of locomotor and manipulative abilities. Science 333, 1411–1417.
Kono, R., 2004. Molar enamel thickness and distribution patterns in extant great apes and humans, new insights based on a 3-dimensional whole crown perspective. Anthropol. Sci. 112, 121–146.
Kono, R., Suwa, G., 2008. Enamel distribution patterns of extant human and hominoid molars: occlusal versus lateral enamel thickness. Bull. Natl. Mus. Nat. Sci. 34, 1–9.
Kono, R., Suwa, G., Tanijiri, T., 2002. A three-dimensional analysis of enamel distribution patterns in human permanent first molars. Arch. Oral. Biol. 47, 867–875.
Laden, G., Wrangham, R., 2005. The rise of the hominids as an adaptive shift in fallback foods: plant underground storage organs (USOs) and australopith origins. J. Hum. Evol. 49, 482–498.
Lucas, P., Constantino, P., Wood, B., Lawn, B., 2008. Dental enamel as a dietary indicator in mammals. Bioessays 30, 374–385.
Macchiarelli, R., Bondioli, L., Falk, D., Faupl, P., Illerhaus, B., Kullmer, O., Richter, W., Said, H., Sandrock, O., Schäfer, K., 2004. Early Pliocene hominid tooth from Galili, Somali region, Ethiopia. Coll. Antropol. 28, 65–76.
Macchiarelli, R., Bondioli, L., Debénath, A., Mazurier, A., Tournepiche, J.-F., Birch, W., Dean, C., 2006. How Neanderthal molar teeth grew. Nature 444, 748–751.
Macho, G., Thackeray, J., 1993. Computed tomography and intercuspal angulation of maxillary molars of Plio-Pleistocene hominids from Sterkfontein, Swartkrans and Kromdraai (South Africa): An exploratory study. Z. Morphol. Anthropol. 261–269.
Macho, G.A., Spears, I.R., 1999. Effects of loading on the biochemical behavior of molars of *Homo*, *Pan*, and *Pongo*. Am. J. Phys. Anthropol. 109, 211–227.
Mackiewicz, P., Wiszniowska, T., Olejniczak, A., Stefaniak, K., Socha, P., Nadachowski, A., 2010. Analysis of dental enamel thickness in bears with special attention to *Ursus spelaeus* and *U. wenzensis* (=*minimus*) in comparison to selected representatives of mammals. In: Nowakowski, D. (Ed.), Morphology and systematics of fossil vertebrates. DN Publisher, Wroclaw, pp. 60–77.
Martin, L., 1983. The relationships of the later Miocene hominoidea. Department of Anthropology, Ph.D. Dissertation, University College London.
Martin, L., 1985. Significance of enamel thickness in hominoid evolution. Nature 314, 260–263.
Mitteroecker, P., Bookstein, F., 2011. Linear discrimination, ordination, and the visualization of selection gradients in modern morphometrics. Evol. Biol. 38, 100–114.
Molnar, S., 1971. Human tooth wear, tooth function and cultural variability. Am. J. Phys. Anthropol. 34, 175–189.
NESPOS database, 2015. Neanderthal Studies Professional Online Service. http://www.nespos.org.
Olejniczak, A., Martin, L., Ulhaas, L., 2004. Quantification of dentine shape in anthropoid primates. Annls. Anat. 186, 479–485.
Olejniczak, A., Gilbert, C., Martin, L., Smith, T., Ulhaas, L., Grine, F., 2007. Morphology of the enamel-dentine junction in sections of anthropoid primate maxillary molars. J. Hum. Evol. 53, 292–301.
Olejniczak, A., Smith, T.M., Feeney, R.N.M., Macchiarelli, R., Mazurier, A., Bondioli, L., Rosas, A., Fortea, J., de la Rasilla, M., Garcia-Tabernero, A., Radovčić, J., Skinner, M.M., Toussaint, M., Hublin, J.-J., 2008a. Dental tissue proportions and enamel thickness in Neandertal and modern human molars. J. Hum. Evol. 55, 12–23.
Olejniczak, A., Smith, T.M., Skinner, M.M., Grine, F.E., Feeney, R.N.M., Thackeray, J.F., Hublin, J.-J., 2008b. Three-dimensional molar enamel distribution and thickness in *Australopithecus* and *Paranthropus*. Biol. Lett. 4, 406–410.
Olejniczak, A., Tafforeau, P., Feeney, R.N.M., Martin, L.B., 2008c. Three-dimensional primate molar enamel thickness. J. Hum. Evol. 54, 187–195.
Pickering, R., Kramers, J.D., Hancox, P.J., de Ruiter, D.J., Woodhead, J.D., 2011. Contemporary flowstone development links early hominin bearing cave deposits in South Africa. Earth Planet. Sci. Lett. 306, 23–32.
R Development Core Team, 2012. R: A language and environment for statistical computing. R Foundation for Statistical Computing, Vienna.
Radovčić, J., Smith, F.H., Trinkaus, E., Wolpoff, M.H., 1988. The Krapina Hominids: An Illustrated Catalog of Skeletal Collection. Mladost and the Croatian Natural History Museum, Zagreb.
Rampont, M., 1994. Les squelettes, os et dents de foetus, nouveaux-nés et enfants du Musée Anatomique de Strasbourg. Aspects historiques et catalogue. Ph.D. Dissertation, Louis Pasteur University.
Rink, W.J., Schwarcz, H.P., Smith, F.H., Radovčić, J., 1995. ESR dates for Krapina hominids. Nature 378, 24.
Robinson, J.T., 1956. The dentition of the Australopithecinae. Trans. Mus. Mem. 9, 1–179.
Rozzi, F.R., 1998. Can enamel microstructure be used to establish the presence of different species of Plio-Pleistocene hominids from Omo, Ethiopia? J. Hum. Evol. 35, 543–576.
Schwarcz, H.P., Grün, R., Tobias, P.V., 1994. ESR dating studies of the australopithecine site of Sterkfontein, South Africa. J. Hum. Evol. 26, 175–181.
Schwartz, G., 2000. Taxonomic and functional aspects of the patterning of enamel thickness distribution in extant large-bodied hominoids. Am. J. Phys. Anthropol. 111, 221–244.
Schwartz, G.T., 1997. Taxonomic and functional aspects of enamel cap structure in South African plio-pleistocene hominids: a high resolution computed tomographic study. Ph.D. Dissertation, Washington University.
Skinner, M.M., 2008. Enamel-dentine junction morphology of extant hominoid and fossil hominin lower molars. Ph.D. Dissertation, George Washington University.
Skinner, M.M., Wood, B.A., Boesch, C., Olejniczak, A.J., Rosas, A., Smith, T.M., Hublin, J.-J., 2008a. Dental trait expression at the enamel-dentine junction of lower molars in extant and fossil hominoids. J. Hum. Evol. 54, 173–186.
Skinner, M.M., Gunz, P., Wood, B.A., Hublin, J.-J., 2008b. Enamel-dentine junction (EDJ) morphology distinguishes the lower molars of *Australopithecus africanus* and *Paranthropus robustus*. J. Hum. Evol. 55, 979–988.
Skinner, M.M., Wood, B., Hublin, J.-J., 2009. Protostylid expression at the enamel-dentine junction and enamel surface of mandibular molars of *Paranthropus robustus* and *Australopithecus africanus*. J. Hum. Evol. 56, 76–85.
Skinner, M.M., Evans, A., Smith, T., Jernvall, J., Tafforeau, P., Kupczik, K., Olejniczak, A.J., Rosas, A., Radovčić, J., Thackeray, J.F., Toussaint, M., Hublin, J.-J., 2010. Brief communication: Contributions of enamel-dentine junction shape and enamel deposition to primate molar crown complexity. Am. J. Phys. Anthropol. 142, 157–163.
Skinner, M.M., Alemseged, Z., Gaunitz, C., Hublin, J.-J., 2015. Enamel thickness trends in Plio-Pleistocene hominin mandibular molars. J. Hum. Evol. 85, 35–45.
Smith, T.M., Martin, L.B., Leakey, M.G., 2003. Enamel thickness, microstructure and development in *Afropithecus turkanensis*. J. Hum. Evol. 44, 283–306.
Smith, T.M., Olejniczak, A.J., Martin, L., Reid, D.J., 2005. Variation in hominoid molar enamel thickness. J. Hum. Evol. 48, 575–592.
Smith, T.M., Olejniczak, A.J., Reid, D.J., Ferrell, R., Hublin, J.-J., 2006. Modern human molar enamel thickness and enamel–dentine junction shape. Arch. Oral. Biol. 51, 974–995.
Smith, T.M., Olejniczak, A.J., Reh, S., Reid, D.J., Hublin, J.-J., 2008. Brief communication: enamel thickness trends in the dental arcade of humans and chimpanzees. Am. J. Phys. Anthropol. 136, 237–241.
Smith, T.M., Olejniczak, A.J., Zermeno, J.P., Tafforeau, P., Skinner, M.M., Hoffmann, A., Radovčić, J., Toussaint, M., Kruszynski, R., Menter, C., Moggi-Cecchi, J., Glasmacher, U.A., Kullmer, O., Schrenk, F., Stringer, C., Hublin, J.-J., 2012. Variation in enamel thickness within the genus *Homo*. J. Hum. Evol. 62, 395–411.
Spencer, M.A., 2003. Tooth-root form and function in platyrrhine seed-eaters. Am. J. Phys. Anthropol. 122, 325–335.
Stricker, D., 2008. BrightStat.com: free statistics online. Comput. Meth. Prog. Bio. 92, 135–143.
Suwa, G., White, T.D., Howell, F., 1996. Mandibular postcanine dentition from the Shungura Formation, Ethiopia: crown morphology, taxonomic allocations, and Plio-Pleistocene hominid evolution. Am. J. Phys. Anthropol. 101, 247–282.
Suwa, G., Kono, R., Katoh, S., Asfaw, B., Beyene, Y., 2007. A new species of great ape from the late Miocene epoch in Ethiopia. Nature 448, 921–924.
Suwa, G., Kono, R., Simpson, S.W., Asfaw, B., Lovejoy, C.O., White, T.D., 2009. Paleobiological implications of the *Ardipithecus ramidus* dentition. Nature 326, 70–99.
Thackeray, J., de Ruiter, D.J., Berger, L.R., van der Merwe, N., 2001. Hominid fossils from Kromdraai: a revised list of specimens discovered since 1938. Annls. Transv. Mus. 38, 43–56.
Thackeray, J., Kirschvink, J.L., Raub, T.D., 2002. Palaeomagnetic analyses of calcified deposits from the Plio-Pleistocene hominid site of Kromdraai, South Africa. S. Afr. J. Sci. 98, 537–540.

Thackeray, J., Braga, J., Sénégas, F., Gommery, D., Potze, S., Senut, B., 2005. Discovery of a humerus shaft from Kromdraai B: part of the skeleton of the type specimen of Paranthropus robustus Broom, 1938? Annls. Transv. Mus. 42, 92–93.

Tobias, P.V., 1978. The earliest Transvaal members of the genus *Homo* with another look at some problems of hominid taxonomy and systematics. Z. Morphol. Anthropol. 69, 225–265.

Ungar, P.S., Grine, F.E., Teaford, M.F., Zaatari, S.E., 2006. Dental microwear and diets of African early *Homo*. J. Hum. Evol. 50, 78–95.

Villmoare, B., Kimbel, W.H., Seyoum, C., Campisano, C.J., DiMaggio, E., Rowan, J., Braun, D.R., Arrowsmith, J.R., Reed, K.E., 2015. Early *Homo* at 2.8 Ma from Ledi-Geraru, Afar, Ethiopia. Science 347, 1352–1355.

Vrba, E.S., 1985. Early hominids in southern Africa: updated observations on chronological and ecological background. In: Tobias, P.V. (Ed.), Hominid evolution: past, present and future. Alan R. Liss, New York, pp. 195–200.

White, T.D., Harris, J.M., 1977. Suid evolution and correlation of African hominid localities. Science 198, 13–21.

White, T.D., Suwa, G., Asfaw, B., 1994. *Australopithecus ramidus*, a new species of early hominid from Aramis, Ethiopia. Nature 371, 306–312.

Wood, B., 2010. Reconstructing human evolution: achievements, challenges, and opportunities. Proc. Natl. Acad. Sci. 107, 8902–8909.

Zanolli, C., 2015. Brief communication: molar crown inner structural organization in Javanese *Homo erectus*. Am. J. Phys. Anthropol. 156, 148–157.

Zanolli, C., Bayle, P., Macchiarelli, R., 2010. Tissue proportions and enamel thickness distribution in the early Middle Pleistocene human deciduous molars from Tighenif, Algeria. C.R. Palevol. 9, 341–348.

Zanolli, C., Bondioli, L., Coppa, A., Dean, C.M., Bayle, P., Candilio, F., Capuani, S., Dreossi, D., Fiore, I., Frayer, D.W., 2014. The late Early Pleistocene human dental remains from Uadi Aalad and Mulhuli-Amo (Buia), Eritrean Danakil: macromorphology and microstructure. J. Hum. Evol. 74, 96–113.